IOP PUBLISHING PLASMA PHYSICS AND CONTROLLED FUSION

Plasma Phys. Control. Fusion **51** (2009) 065023 (13pp) doi:10.1088/0741-3335/51/6/065023

Analysis of turbulence diffusion and H-mode transition in conjunction with gyrocentre shift at the boundary of fusion devices

K C Lee

Department of Applied Science, University of California, Davis, CA 95616, USA

Received 11 July 2008, in final form 16 March 2009
Published 13 May 2009
Online at stacks.iop.org/PPCF/51/065023

Abstract

A new concept of turbulence transport and diffusion coefficient are derived from the microscopic $\tilde{E} \times B$ ($\tilde{E}$ is the localized electric field and $\boldsymbol{B}$ is the magnetic field) drifts at the boundary of fusion devices by characterization of the gyrocentre shift induced by the collisions among electrons, ions and neutrals. It is found that when the viscosity force of the ion–neutral collision is counted, Reynolds numbers of the poloidal ion flow in the vicinity of the tokamak separatrix vary over the critical value between turbulent and laminar flows depending on the plasma parameters such as temperature, neutral density and density fluctuation level, which explains the mechanism of the fast transition from the low confinement mode to the high confinement mode (L/H transition) for the examplar cases.

(Some figures in this article are in colour only in the electronic version)

1. Introduction

One of the most crucial obstacles of nuclear fusion research is that the rate of transport at the boundary of fusion devices is extremely high. This phenomenon is called 'anomalous transport' since it has remained unexplained despite numerous attempts. It is believed that the main difficulty in understanding the transport of magnetized plasma comes from its turbulent feature. The purpose of this paper is to provide a new revenue towards the understanding of plasma transport especially at the boundary of magnetic fusion devices. While the research on the plasma transport made little progress, high confinement mode (H-mode) was discovered [1]. The typical feature of H-mode transition includes a sudden reduction in radiation (D_α) emission on the diverter, formation of the transport barrier that increases the confinement, increase in density and temperature leading to pedestal formation, a sudden reduction in the density fluctuation and an increase in the radial electric field. Among many theories that have tried to explain the mechanism of the H-mode, the suppression of turbulence by $\boldsymbol{E} \times \boldsymbol{B}$ shear is the one that is widely accepted [2]. Even if the $\boldsymbol{E} \times \boldsymbol{B}$ shear is admitted as the cause of

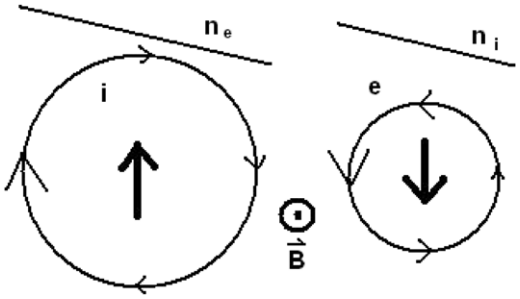

Figure 1. Illustration of gyrocentre shifts by ion–electron collisions. Ions and electrons make collisions while they are moving in each gyro motion. Since the probability of a collision is proportional to the target density, an ion has a net up direction velocity component and an electron has a net down direction velocity component when the average is taken.

the turbulent suppression, the mechanism of the radial electric field formation has remained in question for decades. Recently the gyrocentre shift theory explained the mechanism of the radial electric field formation not only for the typical tokamak boundary [3] but also for the extremely high collision case such as arc discharge with its generalized formula [4]. The fundamental physics of the gyrocentre shift theory is that when there are a significant number of neutrals in the magnetized plasma so that the ions make collisions with neutrals, there exists a poloidal component of ion flow inversely proportional to the neutral density scale length which is perpendicular to both the magnetic field and the direction of the neutral density gradient. Therefore when the poloidal ion flow is counted this term must be added to the other terms such as $\boldsymbol{E} \times \boldsymbol{B}$ drift and the term associated with diamagnetic drift. And when ions make collisions with neutrals these poloidal flow terms transfer to the radial current. In this paper detailed relations of the gyrocentre shift with plasma transport are discussed. In section 2, gyrocentre shift of ion–electron collision and its influence to the plasma transport is discussed. In section 3, plasma transports from ion–neutral and electron–neutral collisions are characterized including the turbulence effect. In section 4, Reynolds number for ion–neutral collisions and its relation to L/H transitions are introduced. The example calculations of a tokamak boundary are presented in section 5 followed by the conclusions.

2. Plasma transport from ion–electron collision

The first paper on the gyrocentre shift [3] was on the basis of the assumption that particle collisions other than ion–neutral are not significant for the charge separation. However the same principle of gyrocentre shift can be applied to other collisions than ion–neutral collisions such as ion–electron collisions and they have an important effect on the particle transport and even for the saturation of charge separation. As indicated in figure 1, ions and electrons have net vertical velocity components due to the target particle density gradient when they are averaged over a circle of gyro-motion (the third terms on the right hand sides of the equations below). When there are collisions, the pressure gradient plays a role for the momentum exchange. Although individual incident particle has no real gyrocentre drift, the target particle experiences an unbalanced influx of incident particles. When these influxes are averaged out the net velocity remains, which has the same magnitude of the diamagnetic drift. So for the final velocity of the incident particle in a collision, firstly the $\boldsymbol{E} \times \boldsymbol{B}$ drift should be included (since each particle has real drift from the electric field), secondly, the term associated with

diamagnetic drift should be included since this velocity component also acts for the momentum exchange. Therefore the average poloidal velocity component of the incident particle at the moment of the collision can be described as follows,

$$\upsilon_{\mathrm{yi}} = -\frac{E}{B} + \frac{kT_{\mathrm{i}}}{qB}\frac{1}{n_{\mathrm{i}}}\frac{\partial n_{\mathrm{i}}}{\partial x} - \frac{kT_{\mathrm{i}}}{qB}\frac{1}{n_{\mathrm{e}}}\frac{\partial n_{\mathrm{e}}}{\partial x},$$
$$\upsilon_{\mathrm{ye}} = -\frac{E}{B} + \frac{kT_{\mathrm{e}}}{eB}\frac{1}{n_{\mathrm{e}}}\frac{\partial n_{\mathrm{e}}}{\partial x} - \frac{kT_{\mathrm{e}}}{eB}\frac{1}{n_{\mathrm{i}}}\frac{\partial n_{\mathrm{i}}}{\partial x},$$

where E is the radial electric field, B is the toroidal magnetic field, kT_{i} is the ion thermal energy, kT_{e} is the electron thermal energy, q is the ion charge, e is the electron charge, n_{i} is the ion density and n_{e} is the electron density. Here the temperature gradient is ignored. In this case the $\boldsymbol{E}\times\boldsymbol{B}$ drift component has no contribution to the momentum exchange at the collision because both particles move at the same velocity. For each species, two terms on the right hand side other than the $\boldsymbol{E}\times\boldsymbol{B}$ drift cancel each other when the density gradient scale lengths for ion and electron are the same ($\frac{1}{n_{\mathrm{i}}}\frac{\partial n_{\mathrm{i}}}{\partial x} \approx \frac{1}{n_{\mathrm{e}}}\frac{\partial n_{\mathrm{e}}}{\partial x}$). Therefore the components described in the above equations make little contribution to the momentum exchange at the ion–electron collision. Only when there is a temperature gradient or other poloidal drift such as grad $\boldsymbol{B}$ drift which is in opposite directions to each other, the effective vertical velocity remains as follows:

$$\upsilon_{\mathrm{yi}} = \frac{kT_{\mathrm{i}}}{qB}\frac{1}{T_{\mathrm{i}}}\frac{\partial T_{\mathrm{i}}}{\partial x} + \frac{kT_{\mathrm{i}}}{qB}\frac{1}{B}\frac{\partial B}{\partial x},$$
$$\upsilon_{\mathrm{ye}} = \frac{kT_{\mathrm{e}}}{eB}\frac{1}{T_{\mathrm{e}}}\frac{\partial T_{\mathrm{e}}}{\partial x} + \frac{kT_{\mathrm{e}}}{eB}\frac{1}{B}\frac{\partial B}{\partial x}.$$

Then the collision of an ion with an electron makes momentum exchange in the range of $m_{\mathrm{e}}\upsilon_{\mathrm{ye}}$ because of the large mass difference between the ion and the electron. Using the fluid equation, $\boldsymbol{J}\times\boldsymbol{B} = n\nu_{\mathrm{i-e}}m_{\mathrm{e}}\upsilon_{\mathrm{ye}}$ ($\boldsymbol{J}$ is the current density, $\nu_{\mathrm{i-e}}$ is the frequency of ion–electron collision and n is the particle density) one can get the horizontal (radial direction in the tokamak geometry) velocity from the current density as follows:

$$\upsilon_{\mathrm{xi}} = \upsilon_{\mathrm{xe}} = -\frac{\nu_{\mathrm{i-e}}m_{\mathrm{e}}}{eB}\frac{kT_{\mathrm{e}}}{eB}\frac{1}{T_{\mathrm{e}}}\frac{\partial T_{\mathrm{e}}}{\partial x} - \frac{\nu_{\mathrm{i-e}}m_{\mathrm{e}}}{eB}\frac{kT_{\mathrm{e}}}{eB}\frac{1}{B}\frac{\partial B}{\partial x} = -\frac{1}{2}\nu_{\mathrm{i-e}}r_{\mathrm{Le}}^2\left(\frac{1}{T_{\mathrm{e}}}\frac{\partial T_{\mathrm{e}}}{\partial x} + \frac{1}{B}\frac{\partial B}{\partial x}\right), \tag{1}$$

where r_{Le} is the electron gyro radius and $n_{\mathrm{i}} = n_{\mathrm{e}}$, $q = -e$ are assumed.

Equation (1) indicates that when there is a temperature gradient or a magnetic field gradient, ion and electron flow down on these gradients. Since both species have the same velocity, they make a plasma transport which is naturally ambipolar. In actual tokamks there are radial electric fields and charge separation so n_{i} is not exactly equal to n_{e}. This would makes equation (1) more complicated, but its transport rate is in the range of the classical diffusion coefficient which is much smaller than the transport described in section 3.3.

3. Plasma transport from ion–neutral and electron–neutral collisions

3.1. Saturation of the radial electric field

The average vertical velocities of an ion and an electron upon collision with a neutral can be described as follows:

$$\upsilon_{\mathrm{yi}} = -\frac{E}{B} + \frac{1}{qB}\frac{1}{n_{\mathrm{i}}}\frac{\partial P_{\mathrm{i}}}{\partial x} - \frac{kT_{\mathrm{i}}}{qB}\frac{1}{n_{\mathrm{n}}}\frac{\partial n_{\mathrm{n}}}{\partial x},$$
$$\upsilon_{\mathrm{ye}} = -\frac{E}{B} + \frac{1}{eB}\frac{1}{n_{\mathrm{e}}}\frac{\partial P_{\mathrm{e}}}{\partial x} - \frac{kT_{\mathrm{e}}}{eB}\frac{1}{n_{\mathrm{n}}}\frac{\partial n_{\mathrm{n}}}{\partial x},$$

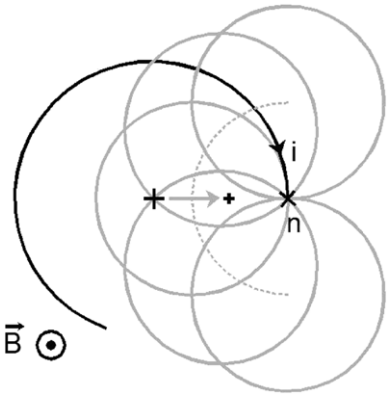

Figure 2. Scattered angle distribution of ion–neutral elastic scattering. From the conservation of energy and momentum, incident ion loses half of its momentum. Here the grey solid lines are trajectories of scattered ions and the dotted line is a trace of their gyrocentres. Taking the average of the scattered gyrocentres makes the gyrocentre shift of an elastic scattering as half of the incident ion gyroradius.

where P_i is the ion pressure and P_e is the electron pressure. While the momentum loss of the ion–neutral charge exchange is $m_\mathrm{i}v_\mathrm{yi}$ because the ion loses its identity and the new ion's direction is isotropic, the ion–neutral elastic scattering makes momentum loss of $1/2m_\mathrm{i}v_\mathrm{yi}$ since the scattered angle distribution is isotropic in the centre of the mass system, as indicated in figure 2. On the other hand, the electron–neutral collisions make momentum loss of $m_\mathrm{e}v_\mathrm{ye}$ because of the large mass difference of the neutral from the electron. Again by the fluid equation of $\boldsymbol{J}\times\boldsymbol{B} = n\nu S^\mathrm{m}$ (ν is the collision frequency and S^m is the momentum loss), the radial current densities are described as follows,

$$J_\mathrm{i}^\mathrm{GCS} = \frac{m_\mathrm{i}n_\mathrm{i}\nu_\mathrm{i-n}}{B}\left(\frac{E}{B} - \frac{1}{qB}\frac{1}{n_\mathrm{i}}\frac{\partial P_\mathrm{i}}{\partial x} + \frac{kT_\mathrm{i}}{qB}\frac{1}{n_\mathrm{n}}\frac{\partial n_\mathrm{n}}{\partial x}\right) \tag{2}$$

$$J_\mathrm{e}^\mathrm{GCS} = -\frac{m_\mathrm{e}n_\mathrm{e}\nu_\mathrm{e-n}}{B}\left(\frac{E}{B} - \frac{1}{eB}\frac{1}{n_\mathrm{e}}\frac{\partial P_\mathrm{e}}{\partial x} + \frac{kT_\mathrm{e}}{eB}\frac{1}{n_\mathrm{n}}\frac{\partial n_\mathrm{n}}{\partial x}\right),$$

where $\nu_\mathrm{i-n} = \nu_\mathrm{c.x.} + 0.5\nu_\mathrm{el}$ ($\nu_\mathrm{c.x.}$ is the charge exchange frequency, ν_el is ion–neutral elastic scattering frequency) and $\nu_\mathrm{e-n}$ is the electron–neutral collision frequency. As indicated above, ion current is higher than electron current approximately by the difference in their masses. Therefore, as time goes by, the ion current makes charge separation by the continuity equation ($\nabla J = -\mathrm{d}\rho/\mathrm{d}t$, ρ is the charge density), and as charge separation increases, the electric field also increases, which is in the opposite direction to the ion current so that the ion current approaches zero. When the charge separation is built in an infinite slab geometry, the resulting electric field is induced by the equation of $\nabla E = \rho/2\varepsilon_0$, where ε_0 is the permittivity of vacuum. By combining this equation with equation (2) and the continuity equation, one can find that the time evolutions of the ion current density and the electric field formation are in the form of exponential decay such as $J(t) = J_0 e^{\frac{-t}{t_0}}$ and $E(t) = E_\infty(1 - e^{\frac{-t}{t_0}})$ where J_0 is J_i when $E = 0$, E_∞ is the steady state electric field and $t_0 = \varepsilon_0 B^2/m_\mathrm{i}n_\mathrm{i}\nu_\mathrm{i-n}$. In typical tokamak boundary conditions t_0 can be as small as a few microseconds. Note that in this analysis

$$\frac{\mathrm{d}E}{\mathrm{d}t}\rangle\rangle - \frac{\mathrm{d}t(\nabla P/qn_\mathrm{i})}{\mathrm{d}t} + \frac{\mathrm{d}(kT_\mathrm{i}\nabla n_\mathrm{n}/qn_\mathrm{n})}{\mathrm{d}t}$$

is assumed and this assumption is agreed to the experimental measurements at H-mode transitions where typical pedestal density rising time is in the range of a few milliseconds.

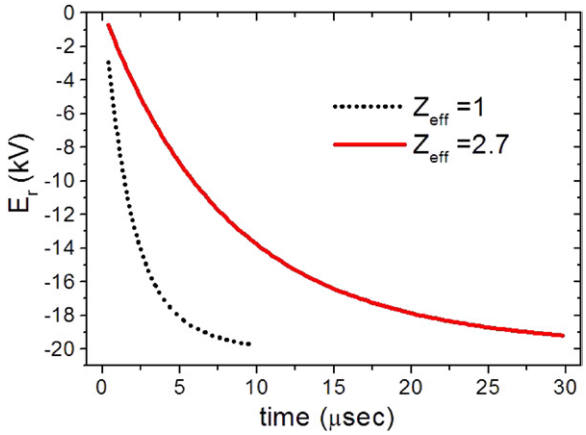

Figure 3. Time evolution of radial electric field formation described by $E(t) = E_\infty(1 - e^{\frac{-t}{t_0}})$, where $t_0 = \varepsilon_0 B^2/m_i n_i \nu_{i-n}$. When Z_{eff} is high n_i becomes small and this makes slower formation of the radial electric field. Usually plasma parameters change continuously so there is no such formation from zero initial value as in the figure; however this scale of time can be a limiting factor for the sudden change at the L/H transition, as indicated in figure 6. This result shows that the coefficient of equation (2) such as n_i and ν_{e-n} does not make a big difference for the saturated value of the radial electric field.

Figure 3 is the time evolution of the radial electric field at a point inside the separatrix when the plasma parameters are simulated for the case of [3].

3.2. No turbulence case

The role of the electron radial current is stopping the charge separation before zero ion current occurs. The saturation condition can be found when the electric field makes the same magnitude of ion current as of the electron current (ambipolar electric field), which is described as follows:

$$m_i n_i \nu_{i-n}\left(E_a - \frac{1}{q}\frac{1}{n_i}\frac{\partial P_i}{\partial x} + \frac{kT_i}{q}\frac{1}{n_n}\frac{\partial n_n}{\partial x}\right) = -m_e n_e \nu_{e-n}\left(E_a - \frac{1}{e}\frac{1}{n_e}\frac{\partial P_e}{\partial x} + \frac{kT_e}{e}\frac{1}{n_n}\frac{\partial n_n}{\partial x}\right),$$

where E_a is the ambipolar electric field. At E_a the ion radial flow rate becomes the same as the electron radial flow so that there is no more charge separation and the electric field is in a steady state. If we assume that ν_{i-n} and ν_{e-n} are the same (they are pretty similar for deuterium plasmas) and $\partial P/\partial x = kT(\partial n/\partial x)$, this flow rate can be described as follows:

$$\upsilon_{xi} = \upsilon_{xe} = \nu_{i-n} r_{Le}^2\left(-\frac{1}{n_i}\frac{\partial n_i}{\partial x} + \frac{1}{n_n}\frac{\partial n_n}{\partial x}\right). \tag{3}$$

Here $n_i = n_e$ and $q = -e$ are assumed. This result shows that the transport from ion collisions with neutrals without turbulence has classical diffusion characteristics again but the magnitude is even smaller than the transport from the electron–ion collision because of the small ion–neutral collision frequency.

3.3. With turbulence case

When there is a turbulent flow in the vicinity of a plasma boundary where the plasma mixes with outside neutrals, the saturation condition of the gyrocentre shift current becomes different

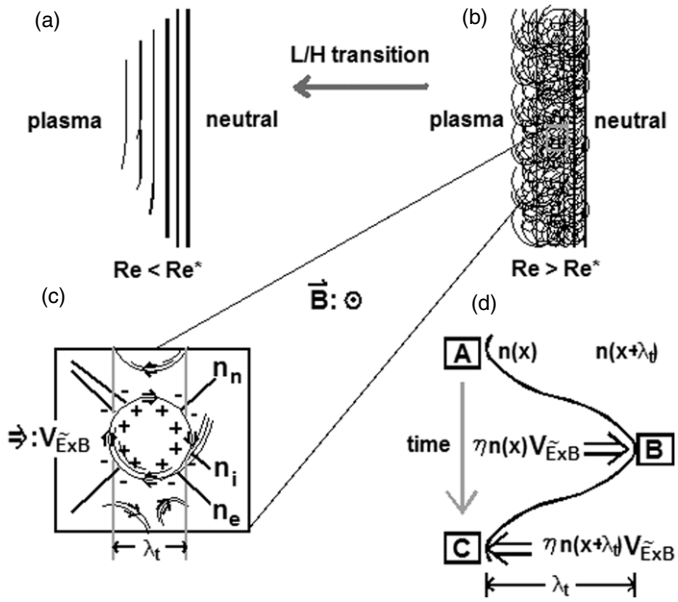

Figure 4. Schematic diagram of the plasma boundary for the turbulence induced diffusion; (*a*) is laminar flow case (H-mode), (*b*) is turbulent flow case (L-mode), (*c*) is a magnified diagram indicating localized turbulent $\tilde{E} \times B$ flows and (*d*) is a diagram of particle flow due to the density fluctuations.

from the case without turbulence. As indicated in figures 4(*b*) and (*c*), when there is a turbulent plasma flow, each bunch of neutrals (neutral-dominant inhomogeneous entity) is generated by turbulence eddy with a cross section on the plane perpendicular to the magnetic field in which the neutrals are concentrated. Since the boundary of this individual bunch has plasma and neutral density gradients (second and third terms on the right hand side of equation (2)), it forms a localized electric field $\tilde{E}$ and an $\tilde{E} \times B$ flow. In the macroscopic view we only count the poloidal contribution from the $\boldsymbol{E} \times \boldsymbol{B}$ flow; however in this microscopic view looking into the individual neutral bunches there are small localized $\tilde{E} \times B$ flows including the radial component. Usually not all the particles are engaged in these $\tilde{E} \times B$ flows so the ratio of the amount engaged in the fluctuation to the whole plasma density can be set as η ($\eta \equiv \tilde{n}/n$). Since the $\tilde{E} \times B$ flow is a convective fluctuation, ions and electrons move around without collision. When the fluctuation scale is λ_t (turbulence wave length), the $\tilde{E} \times B$ flow moving back and forth in the radial direction makes changes in the electron and ion densities as indicated in figures 4(*c*) and (*d*) and table 1.

Here n' denotes $\partial n/\partial x$. When we take a representative value of fluctuation flows moving from x to $x+\lambda_t$, it moves particles corresponding to the amount of $\eta n(x)$ from x to $x+\lambda_t$. And when it moves back from $x+\lambda_t$ to x, it moves the amount of $\eta n\ (x+\lambda_t.)$ from $x+\lambda_t$ to x. After one cycle of representative fluctuation ([A] to [C] in the table 1), particles corresponding to the magnitude of $\eta\lambda_t n'_{i,e}$ move from x to $x+\lambda_t$.; note $0 > n'_i > n'_e$ as indicated in figure 4(*c*) and the same result is obtained from both the left-right-left cycle and the right-left-right cycle. The meaning of setting $0 > n'_i > n'_e$ is that the charge is already separated by the gyrocentre shift (more + charges exist at the right side in figure 4). By the same way of density, the change of charge density after one cycle is summarized as the magnitude of $\eta\lambda_t e(n'_i - n'_e)$ moving from $x+\lambda_t$ to x; here the direction of movement is reversed since $0 > n'_i > n'_e$. This means there is a

Table 1. Turbulence induced transport of plasma and charge.

		x	$x+\lambda_t$
[A]	n	$n_{i,e}(x) \equiv n_{i,e}$	$n_{i,e}(x+\lambda_t) = n_{i,e} + \lambda_t n'_{i,e}$
	ρ	$\rho(x) = e(n_i - n_e) \equiv \rho$	$\rho(x+\lambda_t) = \rho + \lambda_t e(n'_i - n'_e)$
[B]	n	$n_{i,e} - \eta n_{i,e}$	$n_{i,e} + \lambda_t n'_{i,e} + \eta n_{i,e}$
	ρ	$\rho - \eta\rho$	$\rho + \lambda_t e(n'_i - n'_e) + \eta\rho$
[C]	n	$n_{i,e} - \eta n_{i,e} + \eta n_{i,e} + \eta\lambda_t n'_{i,e} + \eta^2 n_{i,e}$ $\approx n_{i,e} + \eta\lambda_t n'_{i,e} = n_{i,e}(x) + \eta\lambda_t n'_{i,e}$	$n_{i,e} + \lambda_t n'_{i,e} + \eta n_{i,e} - \eta n_{i,e} - \eta\lambda_t n'_{i,e} - \eta^2 n_{i,e}$ $\approx n_{i,e} + \lambda_t n'_{i,e} - \eta\lambda_t n'_{i,e} = n_{i,e}(x+\lambda_t) - \eta\lambda_t n'_{i,e}$
	ρ	$\rho(x) + \eta\lambda_t e(n'_i - n'_e)$	$\rho(x+\lambda_t) - \eta\lambda_t e(n'_i - n'_e)$

radial current flow opposite to the current from gyrocentre shift. Here it is worth to noting that the approximation used in table 1 is limited by the first order perturbation and therefore this argument is different from the turbulence structures induced by higher order applications. Now we can continue to discuss the saturation condition of the gyrocentre shift. As charge separation makes progress and the radial current from gyrocentre shift decays, its magnitude becomes the same as the magnitude of radial current from turbulence fluctuation at a point in time. Since these two currents are in opposite directions there is no more charge separation beyond this point (here, electron gyrocentre shift current is neglected). This saturation condition means that the gyrocentre shift current exactly compensates the difference of ion density change from electron density change induced by the turbulence fluctuations (table 1). In the turbulence case, gyrocentre shift only plays the role of saturation of charge separation and major plasma transport comes from the turbulence fluctuations. Each magnitude of electrons and ions moving λ_t of distance is $\eta\lambda_t n'_e$. Note that this is proportional to the electron density gradient not the ion density gradient, and the $\tilde{E} \times B$ flow takes $\pi\lambda_t/v_{\tilde{E}\times B}$ of time to complete one cycle of the circular motion indicated in figures 4(*c*) and (*d*), so the plasma flux moving towards the boundary is described as

$$\Gamma = \frac{\eta}{\pi}\frac{\tilde{E}\lambda_t}{B}n'_e,$$

where $v_{\tilde{E}\times B} = \tilde{E}/B$ is used. This induces the diffusion coefficient as

$$D = \frac{\eta}{\pi}\frac{\tilde{E}\lambda_t}{B}.$$

An approximation for $\tilde{E}\lambda_t$ can be made by the Boltzmann relation; $e\tilde{E}\lambda_t/2 \approx \eta k T_e$ (here the charge separation distance is assumed as $\lambda_t/2$). In this approximation the diffusion coefficient is described as

$$D = \frac{2}{\pi}\eta^2\frac{kT_e}{eB}. \tag{4}$$

For the aspect of diffusion coefficient which is proportional to the square of the density fluctuation level, this result agrees with the experiment where the confinement time is inversely proportional to the square of the density fluctuation level [5].

3.4. Modified Boltzmann relation

It is reported that the Boltzmann relation is not always satisfied in the plasmas. The origin of the Boltzmann relation is that the electric force is in equilibrium with the pressure gradient force. This may be quite true in the core region of tokamaks, but at the boundary there is a

third force acting on the ions. The gyrocentre shift includes poloidal velocities indicated in the parentheses of equation (2). If we call them effective velocity

$$\upsilon^* = \frac{E}{B} - \frac{1}{qB}\frac{1}{n_\mathrm{i}}\frac{\partial P_\mathrm{i}}{\partial x} + \frac{kT_\mathrm{i}}{qB}\frac{1}{n_\mathrm{n}}\frac{\partial n_\mathrm{n}}{\partial x}, \tag{5}$$

the force acting on an ion can be derived by the fluid equation with equation (2);

$$F = \boldsymbol{J}\times\boldsymbol{B} = \frac{m_\mathrm{i}n_\mathrm{i}\nu_{\mathrm{i-n}}}{B}\upsilon^* B = m_\mathrm{i}n_\mathrm{i}\nu_{\mathrm{i-n}}\left(\frac{E}{B} - \frac{1}{qB}\frac{1}{n_\mathrm{i}}\frac{\partial P_\mathrm{i}}{\partial x} + \frac{kT_\mathrm{i}}{qB}\frac{1}{n_\mathrm{n}}\frac{\partial n_\mathrm{n}}{\partial x}\right).$$

In equilibrium the summation of these three force terms is close to zero ($F \approx 0$). By multiplication of parameters for both sides one can get the equation of

$$eE - kT_\mathrm{i}\frac{1}{n_\mathrm{i}}\frac{\partial n_\mathrm{i}}{\partial x} + kT_\mathrm{i}\frac{1}{n_\mathrm{n}}\frac{\partial n_\mathrm{n}}{\partial x} \approx 0$$

(here, $q = e$, $\frac{\partial P_\mathrm{i}}{\partial x} = kT_\mathrm{i}\frac{\partial n_\mathrm{i}}{\partial x}$ are used).

Applying this to the microscopic structure indicated in figure 4(*c*) with an approximation of

$$-\frac{1}{n_\mathrm{n}}\frac{\partial n_\mathrm{n}}{\partial x} \approx \frac{1}{L_{\tilde{n}}}$$

($L_{\tilde{n}}$ is fluctuation density scale length), one can get the force equilibrium equation as follows:

$$\frac{e\tilde{E}}{kT_\mathrm{i}} - \frac{1}{L_{\tilde{n}}} = \frac{1}{n_\mathrm{i}}\frac{\partial n_\mathrm{i}}{\partial x}.$$

By integrating both sides over $\lambda_\mathrm{t}/2$, one can get the modified Boltzmann relation as follows:

$$\frac{\tilde{n}}{n} = \frac{e\tilde{E}\lambda_\mathrm{t}}{2kT_\mathrm{i}} - \frac{\lambda_\mathrm{t}}{2L_{\tilde{n}}}. \tag{6}$$

Regarding that $L_{\tilde{n}}$ becomes small to be comparable with λ_t only at the turbulence dominant region (otherwise $L_{\tilde{n}}$ is larger than λ_t and equation (6) becomes the conventional Boltzmann relation), this result agrees with the experimental measurements of the density fluctuation level and the plasma potential at the boundary of TEXT [6]. Introducing this relation into equation (3) induces the turbulence diffusion coefficient as follows:

$$D = \frac{2}{\pi}\eta\left(\eta + \frac{\lambda_\mathrm{t}}{2L_{\tilde{n}}}\right)\frac{kT_\mathrm{i}}{eB}. \tag{7}$$

4. Reynolds number for ion–neutral collisions and L/H transition.

4.1. Reynolds number of magnetized plasma for collision with neutrals

First of all this concept of Reynolds number which has its origin from ion–neutral collision is different from the magnetic Reynolds number [7] or the parallel viscosity [8] where their origins are from collisions among ions and electrons. When the ion flow with poloidal drift is considered as the main fluid of the friction with neutral, its first different feature from neutral fluid is that the scale length reduces to the ion gyroradius. This is because any ion whose gyrocentre is farther away than its gyroradius from the neutral cannot make a contribution to the friction as indicated in figure 5. The second feature to note is that the magnitude of momentum change that induces the friction is ion mass times the effective velocity which is defined by equation (5). Therefore there is no linear velocity gradient as in the neutral fluid viscosity. When we imagine a thin plate of neutrals located in the middle of a magnetized plasma, apparently this plate experiences viscosity force by collisions of ions (figure 5). The

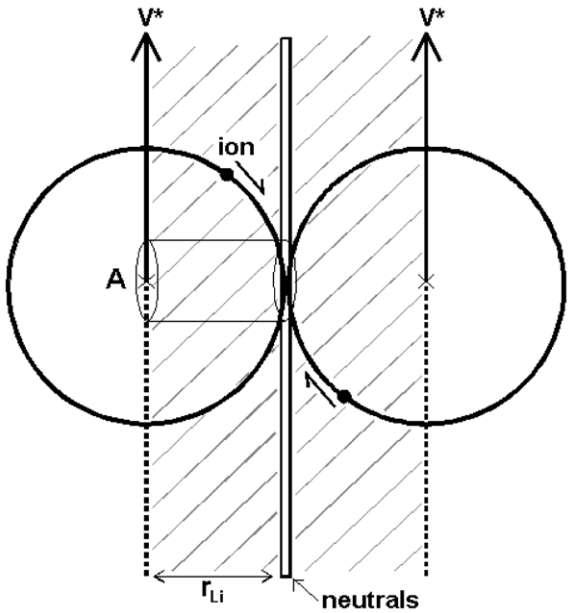

Figure 5. Diagram of the ion viscosity upon neutrals; only ions with gyrocentre located inside the hatched area contribute to the viscosity on the thin layer of neutrals.

viscosity force which is generated by ions in the volume of a cylinder with area of 'A' and height of r_{Li} (indicated in figure 5) is $n_{\mathrm{i}}m_{\mathrm{i}}\nu_{\mathrm{i-n}}\upsilon^{*}Ar_{\mathrm{Li}}$, and the viscosity is defined as $n_{\mathrm{i}}m_{\mathrm{i}}\nu_{\mathrm{i-n}}r_{\mathrm{Li}}^{2}$ from the viscosity force equation ($F_{\theta} = \theta A(\mathrm{d}\upsilon/\mathrm{d}y)$, here $\mathrm{d}\upsilon/\mathrm{d}y = \upsilon^{*}/r_{\mathrm{Li}}$, F_{θ} is viscosity force and θ is viscosity). Reynolds number, which is the ratio of the inertia force to the viscosity force, is described as follows:

$$\mathrm{Re} \equiv \frac{n_{\mathrm{i}}m_{\mathrm{i}}\upsilon^{*2}/r_{\mathrm{Li}}}{n_{\mathrm{i}}m_{\mathrm{i}}\nu_{\mathrm{i-n}}\upsilon^{*}} = \frac{eB}{kT_{\mathrm{i}}}\lambda_{\mathrm{i-n}}\upsilon^{*}, \tag{8}$$

here $\lambda_{\mathrm{i-n}}$ (mean free path of ion-neutral collision) $= 1/\sigma_{\mathrm{i-n}}n_{\mathrm{n}}$, $\nu_{\mathrm{i-n}} = \sigma_{\mathrm{i-n}}\upsilon_{\perp}n_{\mathrm{n}}$, $\sigma_{\mathrm{i-n}}$ is the cross section of ion–neutral collision and $\upsilon_{\perp}$ is the ion velocity perpendicular to the magnetic field.

4.2. Fast and slow changes in L/H transition

As described in section 3.3, the saturation of the radial electric field is determined by the condition that ion gyrocentre shift current cancels the opposite current. When there is turbulent density fluctuation, this condition is described as $(m_{\mathrm{i}}n_{\mathrm{i}}\nu_{\mathrm{i-n}}/B)\upsilon^{*} = D(\partial\rho/\partial x)$, here $\partial\rho/\partial x = e(n_{\mathrm{i}}' - n_{\mathrm{e}}')$. Using this relation together with equations (7) and (8), one can get the Reynolds number as follows:

$$Re = \frac{2}{\pi}\eta\left(\eta + \frac{\lambda_{\mathrm{t}}}{2L_{\tilde{n}}}\right)\frac{B}{m_{\mathrm{i}}n_{\mathrm{i}}(\sigma_{\mathrm{i-n}}n_{\mathrm{n}})^{2}\upsilon_{\perp}}\frac{\partial\rho}{\partial x}. \tag{9}$$

Here the general feature of fluids that the Reynolds number determines critical states from turbulent flow to laminar flow is applied. In an L-mode state, the Reynolds number is higher than the critical Reynolds number ($Re^{*} \sim 2400$) so η stays at a higher value of turbulence. As heating is added, the Reynolds number decreases due to the change of plasma parameters.

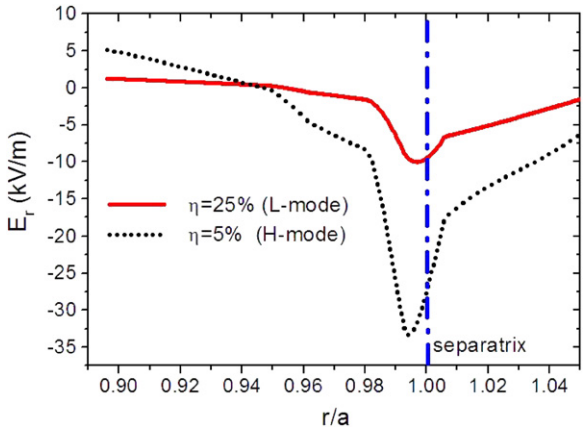

Figure 6. Radial electric field profiles for L-mode and H-mode cases. The calculations are carried out by the uniform density fluctuation level, but the density fluctuation levels in the vicinity of the separatrix are close to the experimental values.

When the Reynolds number reaches Re^*, the turbulence is suppressed and η reduces suddenly, which leads to a further reduction in the Reynolds number. The second change in the L/H transition is the increase in the radial electric field which comes from the change in the saturation condition due to the reduction in η (since the opposite current due to the turbulence is reduced, ion gyrocentre shift current makes a deeper saturation than the L-mode case). This increase in the radial electric field continues as the pressure gradient becomes stiffer, which is the result of turbulence transport decrease by the reduction in diffusion described by equation (7). The direct influences of turbulence suppression are η reduction and turbulence transport decrease; these are the fast changes in the L/H transition. The secondary influence is the increase in the radial electric field, part of which comes from η reduction and part of which comes from the profile change in the plasma pressure which is the slow change of L/H transition triggered by the fast changes. The bifurcation of the L/H transition comes from fast changes since η reduction leads to a further decrease in the Reynolds number. On the other hand, the slow change in the L/H transition is unfavorable to the clear bifurcation since the stiffer density gradient generates a higher Reynolds number (the stiffer density gradient induces the higher radial electric field, which induces an increase in $\partial\rho/\partial x$ in equation (9) and lowering neutral density increases the Reynolds number at the inside of the separatrix). The bifurcation characteristics depend on the amount of η reduction occurring at the transition, therefore if the η reduction at the transition is too small, the Reynolds number can be bounced back to higher than Re^*. In this case, H-mode plasma returns to L-mode after a short period in which the stiff density profile forms. And the reverse process also can occur with multiple cycles of both L/H and H/L transitions. This analysis agrees with the experiments for the aspect that the dithering H-mode occurs when the confinement improvement by transition is marginal [9].

5. Examples of calculations

First, to check the saturation condition of the gyrocentre shift where its current is compensated by the turbulence induced opposite current ($(m_i n_i \nu_{i-n}/B)\upsilon^* = D(\partial\rho/\partial x)$), the profiles of the plasma parameters in the [3] were taken. The calculation results in figure 6 indicate that

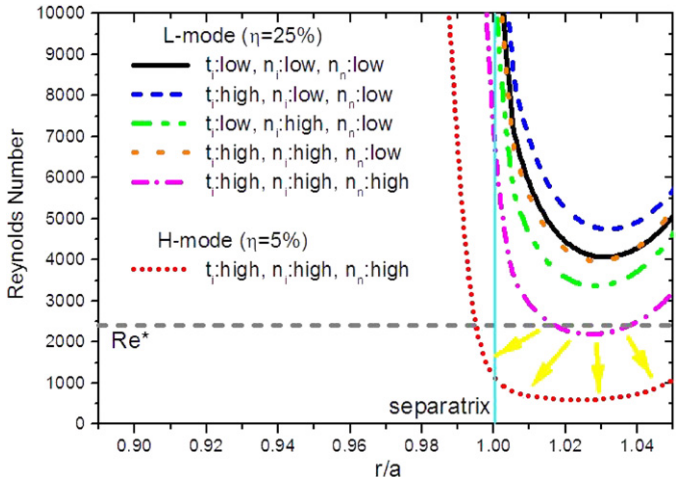

Figure 7. Calculated Reynolds number profiles for different plasma parameters. Grey (yellow) arrows indicate the propagation of laminar region at the moment of L/H transition.

the saturated electric field profile depends largely on the density fluctuation level and if we chose typical density fluctuation levels for the L-mode ($\eta = 25\%$) and H-mode ($\eta = 5\%$), the radial electric field increase immediately after transition by deeper saturation discussed in section 4.2. The magnitude of the saturated radial electric field in figure 6 is in agreement with the experimental comparison in [3]. Basically the same plasma parameter profiles of figure 6 are used for the calculation of Reynolds number profiles with variations of low and high cases and its results are indicated in figure 7. The plasma parameters in figure 7 have a difference of 50% in magnitude for the low and high cases. As indicated in figure 7, if only ion temperature is raised, the Reynolds number would increase. However, the plasma heating process practically induces increases in both ion temperature and ion density and the Reynolds number decreases with ion density. Therefore the overall effect of the plasma heating for the Reynolds number depends on the combination of these two opposite influences. The plasma heating includes the ionization process at the boundary, and the temperature dependence of ionization cross section is very stiff rising at low temperature (up to 40 eV). This means if the neutral gas is sufficiently supplied, the plasma heating not only increases the ion temperature but also induces a high rate of density rising at the boundary. Another strong factor for Reynolds number reduction is the increase in neutral density, which is indicated in figure 7. Although higher neutral density seems to be favourable to the H-mode access, too many neutrals may cool down the plasma and reduce the ion density. This complicated effect of plasma heating and neutral supply is regarded as one of the reasons for the casual access of L/H transition found in the experiments. Figure 7 shows that the range of the Reynolds number of a typical tokamak experiment covers the critical value even though the detail profile effects such as ionization are not counted (the low and high cases in figure 7 are simply taken by uniform changes in the parameters).

6. Discussion and conclusions

One of the reasons that make uncovering the physics of the tokamak boundary so difficult is that there are lots of elements to check out. For example there are high level impurities

at the tokamak boundary and they affect the plasma in many ways. Here we have neglected the effect of gyrocentre shift by impurity ions such as the reaction of C^{+6} and D^0 into C^{+5} and D^+ since its shift of gyrocentre after the reaction is small although the rate coefficient is comparable to the main ion's charge exchange rate coefficient. Another element to check for the gyrocentre shift is the contribution from the banana orbit motion. When a trapped ion makes the reaction with a neutral, the average poloidal momentum loss over the whole banana orbit is non-zero. However, we neglect this effect because the poloidal component of banana motion is slower than the ion thermal velocity and the number of ions engaged in this contribution declines quickly as the neutral density increases since the ratio of the banana orbit radius to the mean free path increases rapidly. Further more passing particles have no contribution especially around the x-point which is regarded as an important region for H-mode triggering. Another issue not included thoroughly in this paper is the mechanism of perpendicular transport in the region outside of the separatrix ; scrape-off-layer (SOL). The diffusion coefficient developed in section 3 (equation (7)) may not be applicable to the SOL since in this region the flux surface is not closed and parallel plasma flow heats the plasma facing components such as the diverter and this changes the equilibrium condition of the radial charge distribution. Lastly, the effect from collisions among ions and electrons such as poloidal viscosity and toroidal rotation is not included here. Although thorough investigations of the issues including those discussed above remain as future work, the following are the conclusions.

(a) The perpendicular particle motion through the gyrocentre shift of electron–ion collisions induces transport as the random walks of the electron gyroradius inversely proportional to the scale lengths of the electron temperature gradient and the magnetic field gradient (equation (1)). The gyrocentre shift of electron–neutral and ion–neutral collisions for the non-turbulence case induces transport as the random walks of electron gyroradius inversely proportional to the scale lengths of the ion density gradient and the neutral density gradient (equation (3)).

(b) When the plasma–neutral collisions are significant and the neutral density gradient is high, the Boltzmann relation needs to be modified to include the force acting from the neutral density gradient to ions (equation (6)).

(c) The turbulence flow generated by the ion-neutral collisions induces diffusive transport (equation (7)) with the saturation condition of the gyrocentre shift current where turbulence induced charge dilation compensates the gyrocentre shift current.

(d) A new concept of the Reynolds number for the magnetized plasma with ion–neutral collisions is introduced (equation (8)) and this Reynolds number represents the plasma state between turbulent and laminar flows as the conventional Reynolds number does for the neutral fluids. As indicated in figure 7 under certain conditions of the plasma parameters around the separatrix, the Reynolds number becomes smaller than the critical value and the turbulence is suppressed. The reduction in the density fluctuation level decreases more of the Reynolds number since it is a function of the density fluctuation level (equation (9)), which provides a candidate explanation of the L/H transitions in fusion devices.

Acknowledgment

The author's sincere appreciation goes to the National Spherical Torus Experiment (NSTX) research team.

References

[1] Wagner F *et al* 1982 *Phys. Rev. Lett.* **49** 1408
[2] Burrell K H 1997 *Phys. Plasmas* **4** 1499
[3] Lee K C 2006 *Phys. Plasmas* **13** 062505
[4] Lee K C 2007 *Phys. Rev. Lett.* **99** 065003
[5] TFR Group and Truc A 1986 *Nucl. Fusion* **26** 1303
[6] Ritz Ch P *et al* 1989 *Phys. Rev. Lett.* **62** 1844
[7] Goldston R J and Lutherford P H 1995 *Introduction to Plasma Physics* (Bristol: Institute of Physics Publishing) p 127
[8] Shaing K C and Callen J D 1983 *Phys. Fluids* **26** 3315
[9] Holzhauer E *et al* 1994 *Plasma Phys. Control. Fusion* **36** A3–11